

Article

A Comparative Study of the Genetic Deep Learning Image Segmentation Algorithms

Wenbo Wang ¹, Muhammad Yousaf ², Ding Liu ^{1,3,*}  and Ayesha Sohail ² ¹ School of Mechano-Electronic Engineering, Xidian University, Xi'an 710071, China² Department of Mathematics, Comsats University Islamabad, Lahore 54000, Pakistan³ Intelligent Robot Laboratory, Hangzhou Institute of Technology, Xidian University, Hangzhou 311231, China

* Correspondence: dliu@xidian.edu.cn

Abstract: Medical optical imaging, with the aid of the “terahertz tomography”, is a novel medical imaging technique based on the electromagnetic waves. Such advanced imaging techniques strive for the detailed theoretical and computational analysis for better verification and validation. Two important aspects, the analytic approach for the understanding of the Schrodinger transforms and machine learning approaches for the understanding of the medical images segmentation, are presented in this manuscript. While developing an AI algorithm for complex datasets, the computational speed and accuracy cannot be overlooked. With the passage of time, machine learning approaches have been further modified using the Bayesian, genetic and quantum approaches. These strategies have boosted the efficiency of the machine learning, and specifically the deep learning tools, by taking into account the probabilistic, evolutionary and quantum qubits hypothesis and operations, respectively. The current research encompasses the detailed analysis of image segmentation algorithms based on the evolutionary approach. The image segmentation algorithm that converts the color model from RGB to HSI and the image segmentation algorithm that uses the clustering technique are discussed in detail, and further extensions of these genetic algorithms to quantum algorithms are proposed. Based on the genetic algorithm, the optimal selection of parameters is realized so as to achieve a better segmentation effect.

Keywords: genetic algorithm; medical image segmentation; skin disease; clustering technique; Schrodinger transform



Citation: Wang, W.; Yousaf, M.; Liu, D.; Sohail, A. A Comparative Study of the Genetic Deep Learning Image Segmentation Algorithms. *Symmetry* **2022**, *14*, 1977. <https://doi.org/10.3390/sym14101977>

Academic Editor: Sergei D. Odintsov

Received: 27 July 2022

Accepted: 14 September 2022

Published: 21 September 2022

Publisher's Note: MDPI stays neutral with regard to jurisdictional claims in published maps and institutional affiliations.



Copyright: © 2022 by the authors. Licensee MDPI, Basel, Switzerland. This article is an open access article distributed under the terms and conditions of the Creative Commons Attribution (CC BY) license (<https://creativecommons.org/licenses/by/4.0/>).

1. Introduction

Medical imaging research has progressed, and novel computational approaches have been used in the literature over the past two decades. The quantum machine learning and the neural network-based quantum-inspired deep learning approaches have attracted the attention of researchers over the past decade due to their novelty and promising cutting-edge applications.

The limitations of deep learning, based on the GPU hard drive and the parallel computers expense, can now be resolved in the coming years with the advancement in the field of quantum deep learning, where the quantum routine is used to transform the classical data to the quantum state, and after the quantum operations, the classical data are retrieved.

Machine learning has served as a useful tool in the field of medical image analysis and in developing smart toolboxes such as radiomics for the image classification. The image segmentation is an important step prior to the image classification. The deep learning approaches have been improved and extended over the past years to segment the images for better analysis and diagnosis in the field of radiology.

The image segmentation has certain limitations. These limitations are discussed in the next section, and such limitations can be removed/overcome with the aid of the smart

genetic algorithms as well as the quantum approaches, where the quantum computing clouds or the quantum models can be used [1–3].

1.1. Historical Background of the Genetic Algorithms for Segmentation

As health problems gradually become the common concern of human beings all over the world, the development of medicine is facing serious challenges. Medical images, which play an important role in medical diagnosis, are also booming. Since medical images are affected by imaging equipment, local volume effects, etc., problems such as edge blurring are inevitable. It is precisely because of the particularity of medical images that image processing technology for medical images has become a highly applicable subject and has developed rapidly. Image segmentation technology is a problem waiting to be solved in the field of medical image processing. Medical image segmentation has a wide range of applications and research value in the field of medical image research. Extracting valuable regions in medical images through segmentation technology can achieve the purpose of facilitating the analysis and identification of medical images [4]. In addition, the use of image segmentation technology to measure the size or volume of human organs, tissues and lesions, so as to achieve disease analysis during the treatment process, can help doctors make a more favorable diagnosis plan for the patient's condition.

Image segmentation is an important part of the field of image processing. It divides an image into several specific regions with unique properties according to certain rules, and each region has similar properties, such as grayscale, color, texture, and contrast. However, in different regions, similar properties show significant differences [5–14]. In general, there is at least one region containing the object of interest in meaningful image segmentation results.

The genetic algorithm is a group-based meta-heuristic algorithm, which draws on the evolutionary laws of the biological world, namely Darwin's natural selection and Mendel's theory of genetic variation: the evolution of organisms is achieved through reproduction, mutation, competition and selection. The genetic algorithm is a random search method based on the above biological model [15]. It was first proposed by Professor J. Holland in the United States in 1975. It has been widely used in machine learning, signal processing and artificial intelligence, and it is one of the key technologies of computing.

The genetic algorithm (GA) represents the solution of a problem as a "chromosome", which is represented in the algorithm as a string encoded in a certain way. Before running the genetic algorithm, some "chromosomes" will be set as candidate solutions to the problem. After that, these "chromosomes" are selected in the "environment" of the problem according to the principle of "survival of the fittest" so as to obtain "chromosomes" that are more suitable for the environment than others to replicate and then let the "chromosomes" carry out crossover, mutation, and obtain a new batch of "chromosomes". These "chromosomes" are more adaptable to the environment than the previous generation. According to such steps, the "chromosome" evolves continuously, and eventually, a "chromosome" group that is most suitable for the environment will be converged, and this "chromosome" group is the optimal solution of the problem. Among them, the ability of the "chromosome" to adapt to the environment is judged by calculating the fitness value of each individual in the group and then selecting the individual to enter the next generation through certain rules (such as the roulette selection mechanism) [16].

There are two main directions for using genetic algorithms in medical image segmentation. One is to use the genetic algorithm to segment the pixel values of the original image, and the other is to combine the genetic algorithm with other algorithms such as neural networks and use the genetic algorithm to iterate the parameters in the network to obtain the optimal parameters.

1.2. Challenges in Medical Image Segmentation

After more than 20 years of development, the image data in the medical field have grown significantly, and there is a lot of information in the image, so extracting this

information has become a difficult problem. At present, many image processing algorithms have been developed to extract the information contained in a large number of medical images, and these algorithms have excellent performance in terms of accuracy, reliability and processing speed. However, the current medical image processing technology still has new challenges [17].

First of all, in the medical field, the clinical conditions of different patients are different, and with the continuous development of medical image technology, more and more medical image analysis technologies are applied to commercial products, which is very important for medical image processing technology. Its applicability presents challenges, requiring it to meet more clinical situations. However, given the complexity of medical conditions and the circumstances of commercial operations, it is not realistic to develop entirely new algorithms for every commercial product. Therefore, for the industrial field, efficiently developing an algorithm and validating the solution is the top priority, which also means achieving success in a short period of time with the least cost. This requires that the framework of the algorithm can be applied to most medical application scenarios.

Finally, when performing algorithm verification, it is necessary to formulate appropriate verification indicators to evaluate whether the algorithm can well accomplish the design goals. Therefore, formulating suitable verification metrics is also one of the challenges. For example, Hicks expounded in his paper the calculation formulas for pixel accuracy, precision, recall, Dice, IoU and other indicators to indicate whether the algorithm segmentation effect is good or not, so indicators are also needed to evaluate when designing algorithms, and different indicators will represent the algorithm performance in different aspects.

To sum up, when designing an image segmentation algorithm for medical images, the first thing to consider is the scope of application of the algorithm, solve problems in a certain field, and then focus on the accuracy, reliability, robustness, and memory of the algorithm. In terms of consumption and calculation time, certain indicators also need to be met. In terms of datasets, it is also a challenge to need enough labeled images to test the algorithm. After that, the algorithm should have the ability to process heterogeneous image data.

2. Materials and Methods

The current research work is divided into two parts: in the first part, we have worked on the application of the leading governing equation, i.e., the Schrodinger equation, in the field of computational radiology, and in the second part, we have worked on the image segmentation of the medical images. The two approaches are used since in the field of quantum mechanics, these two approaches are used in coordination repeatedly [18–20].

The mathematical description of optical solitons is well documented by the nonlinear Schrödinger equation (NLSE). The space time-dependent pulse envelope $\chi(x, t)$, with group velocity dispersion and the self phase modulation, can be better interpreted with the aid of the following one-dimensional model:

$$i\chi_x - \frac{s}{2}\chi_{tt} + N^2|\chi|^2\chi = 0, \quad (1)$$

where $s = \text{sgn}(\mu_2)$, and μ_2 is defined as “second-order-dispersion” effects for the normal and the anomalous GVD. The values can be categorized as follows:

$$s = \text{sgn}(\mu_2) = \begin{cases} 1 & +ve \text{ GVD} \\ -1 & -ve \text{ GVD} \end{cases} \quad (2)$$

Several analytical, semi-analytical and numerical approaches are available in the literature to solve the nonlinear Schrodinger equations, wave equations and numerous types of differential equation, emerging in the field of quantum mechanics, imaging and other fields of applied physics [21], since the mathematical modeling of problems arising in applied sciences can help to forecast the dynamics [22–25], interpret the experimental findings [26–29], and suggest possible solutions to complex nonlinear perturbations [30].

Very recently, the Schrodinger transform method has been used for the medical images and has thus provided a benchmarking tool to this field [31,32].

Similarly, the Schrodinger filters are used in the literature to improve the results of the image segmentation [33].

The nonlinear wave-like phenomena is also present in normal and anomalous GVD, pulse-like solitons.

We will use a spectral method to simulate the two cases. We will first simulate Equation (1) for pulse-like solitons (bright solitons) and then use the two types of dark solitons (black and gray). Now, using the space-time transformation we obtain

$$i\chi_t + \frac{c_0^3}{2}\chi_{xx} + c_0N^2|\chi|^2\chi = 0, \quad (3)$$

where c_0 is the phase speed.

The Caputo fractional derivative $D_t^\alpha\phi$ of order $0 < \alpha \leq 1$ of $\chi : \mathbb{R}_+ \rightarrow \mathbb{R}$ is defined by

$$D_t^\alpha\phi(x, t) = \frac{1}{\Gamma(1-\alpha)} \int_0^t (t-s)^{-\alpha}\phi'(x, s)ds,$$

provided the expression on right-hand side is defined.

We will now introduce the fractional order derivative in time in the Caputo sense and solve the equation by using the Optimal Homotopy Analysis Method.

$$iD_t^\alpha\chi + \frac{c_0^3}{2}\chi_{xx} + c_0N^2|\chi|^2\chi = 0. \quad (4)$$

with the initial condition

$$\chi(x, 0) = Nx$$

Next, the fractional order will be solved with the aid of the Optimal Homotopy Analysis Method. Here, by taking into account the term in absolute form, the main equation can be written as:

$$D_t^\alpha\chi - i\frac{c_0^3}{2}\chi_{xx} - ic_0N^2\chi^2\bar{\chi} = 0 \quad (5)$$

with the initial condition

$$\chi(x, 0) = Nx$$

Choose the linear operator

$$L\{\phi(x, t, q)\} = \frac{\partial^\alpha\phi(x, t, q)}{\partial t^\alpha} \quad (6)$$

with $L\{c\} = 0$ where c is arbitrary constant and the nonlinear operator is defined as

$$\mathcal{N}\{\phi(x, t, q)\} = \frac{\partial^\alpha\phi}{\partial t^\alpha} - i\frac{c_0^3}{2}\frac{\partial^2\phi}{\partial x^2} - ic_0N^2\phi^2\bar{\phi}. \quad (7)$$

The 0th-order deformation equation

$$(1-q)L\{\phi(x, t, q) - \chi_0(x, t)\} = q\hbar H(t)\mathcal{N}\{\phi(x, t, q)\} \quad (8)$$

and

$$\phi(x, t, 0) = \chi_0; \quad \phi(x, t, 1) = \chi(x, t) \quad (9)$$

Now, the m -th order deformation equation is

$$L\{\chi_m(x, t) - \chi_m\chi_{m-1}(x, t)\} = \hbar H(t)R_m(\chi_{m-1}) \quad (10)$$

where

$$R_m(\chi_{m-1}) = \frac{\partial^\alpha \chi_{m-1}}{\partial t^\alpha} - \frac{ic_0^3}{2} \frac{\partial^2 \chi_{m-1}}{\partial x^2} - ic_0 N^2 \sum_{i=0}^{m-1} \sum_{j=0}^i \chi_j \chi_{i-j} \overline{\chi_{m-1-i}} \quad (11)$$

Choose $H(t) = 1$. Now, the solution of Equation (10) becomes

$$\chi_m(x, t) = \chi_m \chi_{m-1}(x, t) + \hbar J^\alpha R_m(\chi_{m-1}) \quad (12)$$

The analytic approximate 0th, first and second-order solutions are

$$\chi_0(x, t) = Nx \quad (13)$$

$$\chi_1(x, t) = -\hbar N c_0 i \left\{ \frac{c_0^2}{2} x + (c_0^2 + N^4)^3 x \right\} \frac{t^\alpha}{\Gamma(1+\alpha)} \quad (14)$$

Similarly

$$\begin{aligned} \chi_2(x, t) = & -(1 + \hbar) \hbar N c_0 i \left\{ \frac{c_0^2}{2} + (c_0^2 + N^4)^2 x \right\} x \frac{t^\alpha}{\Gamma(1+\alpha)} - \frac{N \hbar c_0^4}{2} \\ & \times \left\{ \left\{ \frac{c_0^2}{2} + 3(c_0^2 + N^4)^2 x \right\} (1 + 2x) x + \frac{4N^4}{c_0^2} \left\{ \frac{c_0^2}{2} + (c_0^2 + N^4)^2 x \right\} \right\} \\ & \times 3x \frac{t^{2\alpha} \Gamma(1+\alpha)}{\Gamma(1+2\alpha)} + \hbar c_0^2 N^5 x \left\{ \frac{c_0^2}{2} + (c_0^2 + N^4)^2 x \right\} \frac{t^{3\alpha} \Gamma(1+2\alpha)}{\Gamma(1+3\alpha)} \end{aligned} \quad (15)$$

The convergence can be controlled by minimizing the square residual error

$$\Delta(\hbar) = \int_{\Omega} \left\{ \mathcal{N} \sum_{i=0}^M \chi_i(\tau) \right\}^2 d\tau \quad (16)$$

as $M \rightarrow \infty$, $\Delta(\hbar) \rightarrow 0$.

In the next section, we will focus on the comparative analysis of the numerical algorithms that are suitable for image segmentation.

2.1. Two Algorithms for Image Segmentation

Various algorithms have been reported, reproduced and revisited over the past few decades for medical image analysis, segmentation and exploration [6,13,34]. During this research, two algorithms are compared for accuracy. The first algorithm was proposed by Lei Tang et al. [35], where the researchers developed a machine vision-based weed detection technique and demonstrated an idea of applying genetic algorithms to image segmentation. A strategy of converting the RGB color model to the HSI color model for processing was adapted. Hue–Saturation–Intensity (HSI) [36] is a common color model that separates luminance components from color information and characterizes colors with three basic feature quantities: hue, saturation and intensity [37]. In this color model, H (Hue) is related to the frequency domain characteristics of light and is used to express people's feelings about different colors, and S (Saturation) represents the purity of the color. Saturation is positively related to the vividness of the color. I (Intensity) corresponds to the image brightness or image grayscale, indicating the brightness of the color. RGB color space can be converted to HSI color space by the following Formulas (17)–(19):

$$H = \cos^{-1} \left[\frac{\{(R - G) + (R - B)\}/2}{\sqrt{(R - G)^2 + (R - B)(G - B)}} \right] \quad (17)$$

$$S = 1 - \frac{3}{(R + G + B)} [\min(R, G, B)] \quad (18)$$

$$I = \frac{1}{3}(R + G + B) \quad (19)$$

In this algorithm, to simplify the threshold segmentation method, the distribution in HSI space was examined.

The upper and lower boundaries of HSI are used as the total search space, and each boundary has 256×256 combinations, so there are 256^6 combinations in total. The structure of chromosomes is assigned as upper hue boundary, lower hue boundary, upper saturation boundary, lower saturation boundary, upper and lower intensity boundary. The population size is 48, the championship mode is used for selection, single-point crossover (crossover probability: 0.8), mutation probability: 0.03. At the same time, constraints are added according to the HSI model: all upper boundaries must be greater than their corresponding lower boundaries; otherwise, the correction operation is performed. The fitness values are the weighted values FB and FE of Seno and Senb.

This algorithm has three stopping conditions:

1. The parameter set is higher than the best fitness value of the predefined acceptance threshold;
2. The optimal fitness of the population fails to improve for five consecutive generations;
3. The number of iterations is greater than 100.

The results depict that GAHSI removes a certain number of pixels in low-saturation and low-intensity areas, which means that there is an area in the HSI color space where most plant pixels exist regardless of changes in lighting conditions.

In contrast, another clustering image segmentation algorithm based on genetic algorithm [38] exists. The basic idea of clustering algorithm is as follows:

Suppose the sample set is to be divided into k categories [39].

1. At the beginning, randomly select k points from the sample set $D = \{X_1, X_2, \dots, X_m\}$ as the initial clustering centers of the k categories;
2. In the i th iteration, for any sample point, find the distance to the k centers of the cluster, and assign the sample point to the class of the cluster center with the shortest distance;
3. Use the genetic algorithm to update the cluster center of this class;
4. For all k cluster centers, if the value remains the same or the difference is small after updating by the iterative method of 2, 3, the iteration ends; otherwise, the iteration continues [40].

In this algorithm, four cluster centers are selected, and the genetic algorithm is performed on these four cluster centers. In each generation, for any sample point, it is classified to the nearest cluster center, and then, the cluster center is continuously updated through the genetic algorithm. After continuous iteration, each pixel of the image is assigned to the cluster center to achieve image segmentation [36].

Ultimately, both algorithms achieve image segmentation. Tang et al. compared their algorithm with other clustering algorithms and found that the GAHSI algorithm achieves comparable performance to methods based on clustering algorithms for image segmentation, but GAHSI is more suitable for use in the context of the paper (i.e., under different lighting conditions and weed image segmentation).

A comparison of both algorithms is presented in Figure 1 with the aid of flow charts.

2.2. Datasets

This paper will verify the segmentation effect of the two algorithms on medical images, and then, it will compare and analyze the segmentation performance of the two algorithms through the segmentation results. Therefore, it is necessary to select an appropriate medical image dataset to obtain the comparison results smoothly. Two datasets are selected here; one is the Kvasir-SEG dataset [41]. Polyps are precursors to colorectal cancer; therefore, early automatic detection of more polyps plays a critical role in preventing and surviving colorectal cancer. This was the main motivation for developing the polyp segmentation dataset. The Kvasir-SEG dataset contains 1000 polyp images from Kvasir Dataset v2 and their corresponding ground truth. The images contained in Kvasir-SEG vary in resolution from 332×487 to 1920×1072 pixels.

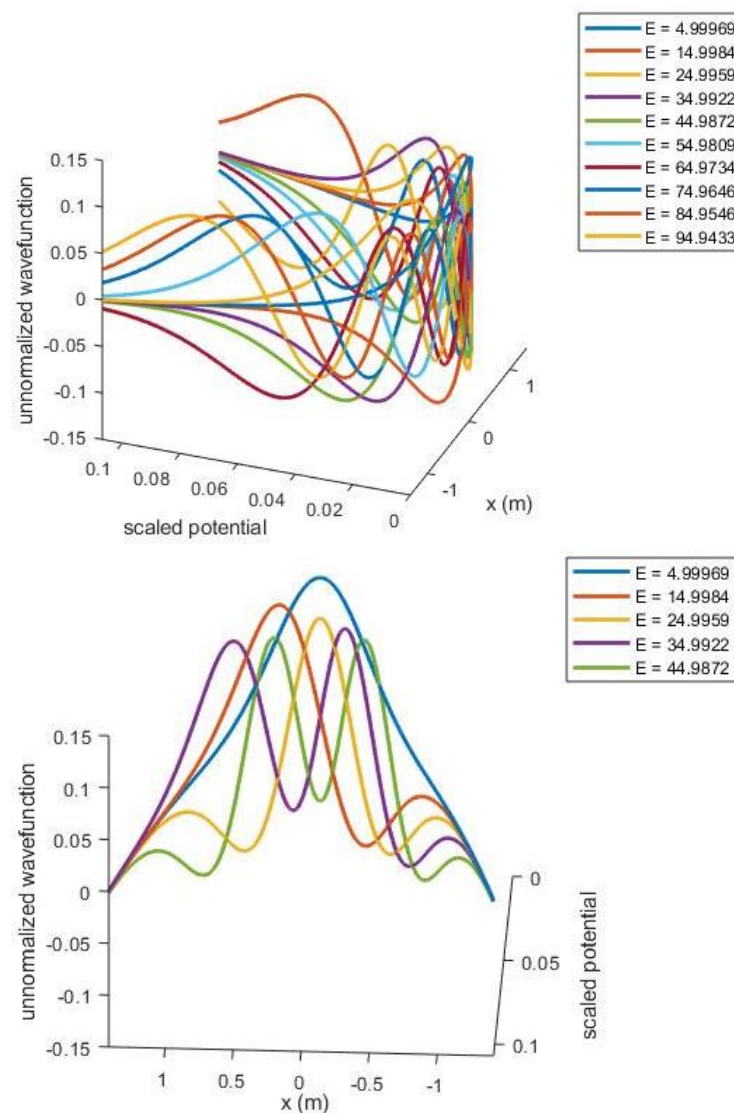


Figure 1. Schrodinger equation solutions to understand the evolution of quantum particles for “terahertz tomography” application.

Next, the ISIC dataset [42,43], published by the International Skin Imaging Collaboration (ISIC), as a large-scale dataset of dermoscopy images, was used to run the numerical experiments. This dataset contains examples of both malignant and benign skin lesions. Each example contains an image of the lesion, and segmenting the lesion and normal areas in the skin will be of great benefit in judging the condition.

3. Results and Analysis

3.1. Results of Methods

The segmentation effects of the two algorithms are evaluated by applying them on two selected datasets. During this process, 20 images were selected for each dataset for validation. No random selection was taken here, but some images were specially selected by manual browsing. In the Kvasir-SEG dataset, because some pictures have some texts that record shooting information, and some of these texts directly overlap with the segmentation target, which may have a certain impact on the segmentation results, a total of 20 of these pictures were selected for use to verify the algorithm. In the ISIC dataset, the diseased tissue of some pictures is occluded by human hair, which will also have a non-negligible impact on the segmentation results. Therefore, five of the 20 pictures selected here are

not occluded by hair, and the diseased tissue is completely exposed, while the rest of the images, especially the diseased tissue, are occluded by hair.

In the process of verification, the original image is first processed by the algorithm that needs to be verified to generate the segmentation result, and then, the result is compared with the manually segmented images in the dataset, and the number of pixels different from the pixel value of the manual segmentation result is calculated. Then, we calculate its proportion in the whole picture to obtain the accuracy and error rate. After completing the processing of 20 images of each dataset, we calculate the mean of its accuracy and error rate and record it in the table.

The performance of the genetic algorithm-based clustering and segmentation algorithm in the two datasets is shown in Table 1 and the schematic is presented in Figure 2. It can be seen that its accuracy in the Kvasir-SEG dataset is only 78.52%. Figures 3 and 4 shows the segmentation result of one of the images. The left image is the original image to be segmented, the middle image is the manually segmented reference image, and the right image is the segmentation result. In the ISIC dataset, the accuracy rate is 86.89%. The segmentation results of one of them are also shown in Figure 4. Then, after converting the RGB images in the dataset to the HSI color model, image segmentation is performed. The performance on the two datasets is shown in Table 2. Here, the same images as the cluster segmentation algorithm are also selected for display (Figures 5 and 6), and these are used to compare the differences.

Table 1. Clustering Segmentation Based on GA.

| Dataset | Accuracy | Error |
|------------|----------|--------|
| Kvasir-SEG | 78.52% | 21.48% |
| ISIC2018 | 86.89% | 13.12% |

Table 2. HSI Segmentation Based on GA.

| Dataset | Accuracy | Error |
|------------|----------|--------|
| Kvasir-SEG | 81.27% | 18.73% |
| ISIC2018 | 81.05% | 19.75% |

3.2. Result Analysis

For the GA-based clustering segmentation algorithm for the dataset Kvasir-SEG, the shooting information has a certain influence on the segmentation effect.

On the other hand, while processing the dataset ISIC, the segmentation results showed that the occlusion of hair has a serious impact on the results. The more serious the occlusion, the worse the segmentation effect.

Next, with the aid of the second algorithm on the first dataset, the HSI-based image segmentation algorithm, through the analysis of the results, it can be found that using the HSI color model for image segmentation, in the Kvasir-SEG dataset, the average accuracy rate is higher than that of cluster segmentation, but the area that should be the background will still be incorrectly segmented.

However, in the ISIC dataset, although the average accuracy rate is lower than cluster segmentation, from the segmentation results, the HSI color model weakens the influence of hair on the pathological area, and the segmented area is closer to the mask, which is more conducive to determining the actual situation of the disease.

Clustering statistics is presented in Table 1 and error analysis is presented in Table 2.

In general, by comparing the performance of the two algorithms on the two datasets, it can be found that on the Kvasir-SEG dataset, the segmentation accuracy of the HSI-based segmentation algorithm is slightly higher than that of the clustering segmentation algorithm. However, according to the actual results of segmentation, the performance of the two types of image segmentation algorithms is equivalent, and both can segment most

of the polyps on the original image. On the ISIC dataset, the segmentation accuracy of the clustering segmentation algorithm is better than that of the HSI-based segmentation algorithm. From the segmentation results, most of the lesion areas can be segmented, while the HSI-based segmentation technology has some lesions.

Even though the algorithms were designed for the segmentation of images, the two algorithms differ greatly in “segmentation details”. The principle of the segmentation algorithm based on clustering technology is simple, but from its performance on the ISIC dataset, it is more susceptible to interference from other factors (the human hair in this database), which shows that a disadvantage of clustering segmentation is that it does not take into account the interaction between adjacent pixels [35]. The HSI-based segmentation technology converts the RGB color model to HSI (as shown in Figures 7 and 8 respectively).

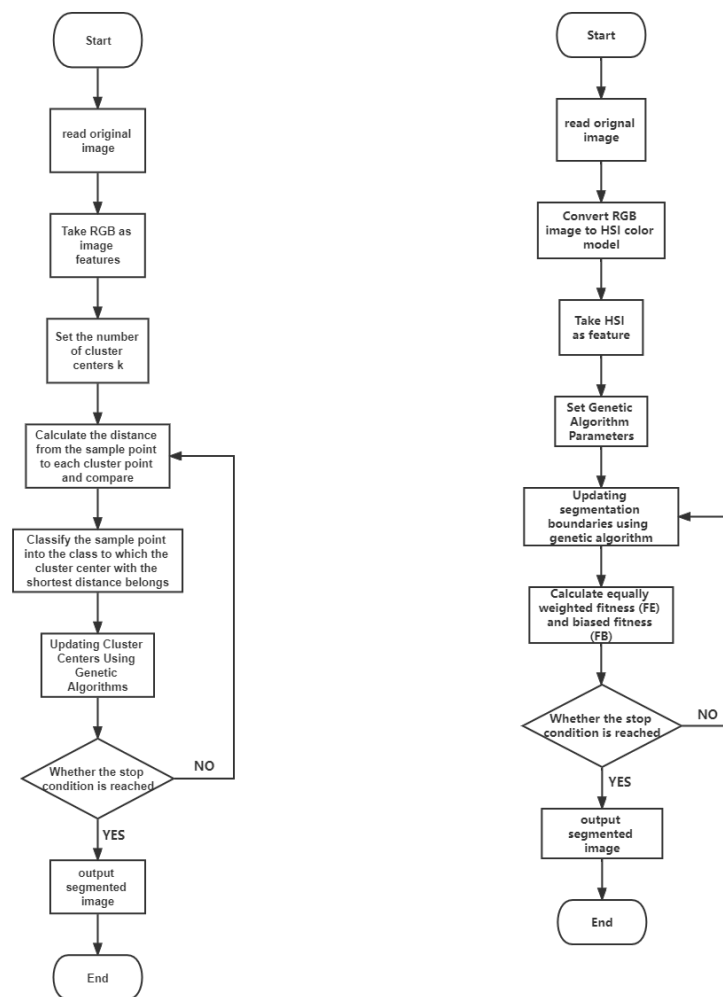


Figure 2. Left: The flow chart of the GA-clustering segmentation algorithm; right: the flow chart of the GA-segmentation algorithm based on the RGB color model.



Figure 3. Segmentation results of the clustering algorithm. The left image is the original image, and the right image is the segmented image.



Figure 4. GA in Kvasir-SEG segmentation results. The left image is an original image of the Kvasir-SEG dataset (curtsy of [42–44]), the middle image is a manually segmented mask for reference, and the right image is a GA-based clustering algorithm.

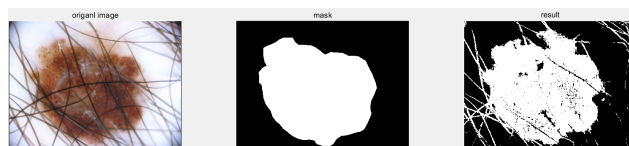


Figure 5. Segmentation results of clustering segmentation based on GA in ISIC. The left image is an original image of the ISIC dataset, the middle image is a manually segmented mask for reference, and the right image is an image segmented using a GA-based clustering algorithm.



Figure 6. GA in Kvasir-SEG results. The left picture is an original image of the Kvasir-SEG dataset, the middle picture is a manually segmented mask for reference, and the right picture is an image segmented using the GA-based HSI.

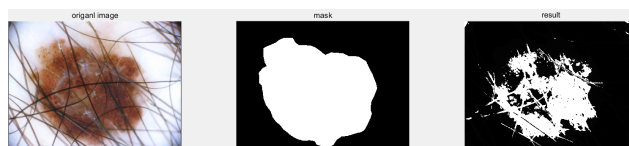


Figure 7. HSI segmentation based on GA in ISIC results. The left picture is an original image of the ISIC dataset, the middle picture is a manually segmented mask for reference, and the right picture is an image segmented using the GA-based HSI algorithm.

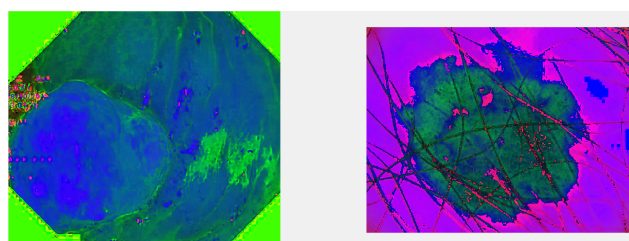


Figure 8. A picture of the HSI color model. Images converted (from two datasets) from RGB to HSI. The left image is the conversion result of the image displayed in the Kvasir-SEG dataset, and the right image is the conversion result of the image displayed in the ISIC dataset.

4. Conclusions

This paper mainly introduces the importance of medical image segmentation in medical image processing as well as the historical background of genetic algorithms and the challenges faced by medical image processing technology today. The principles of the two image segmentation techniques based on genetic algorithms are compared, and they are applied to two medical image datasets, respectively. According to the numerical value of the experimental results and the analysis of the output picture, the performance of the genetic algorithm-based clustering segmentation, and the segmentation technology that

converts the color model to HSI on two datasets, the segmentation effect of the two algorithms is analyzed in detail. The segmentation effects of the two algorithms are equivalent. The GA-based clustering algorithm has a simple principle, while the genetic segmentation algorithm that converts the image to the HSI color model handles the details of the segmentation better. However, it can be seen that the effect of genetic algorithms on the optimization of the algorithm is obvious. In the future, more genetic algorithms can be introduced into medical image segmentation technology to optimize algorithm parameters, thereby improving the applicability of the algorithm to different medical image datasets.

Author Contributions: W.W. did numerical analysis, M.Y. did critical analysis, D.L. did literature review, A.S. did theoretical analysis, all the authors equally contributed in the preparation of the manuscript. All authors have read and agreed to the published version of the manuscript.

Funding: This work was supported in part by the Fundamental Research Funds for the Central Universities under Grant Nos. JB210402 and XJS210406, the Shaanxi Provincial Natural Science Foundation under Grant No. 2021JQ199, the Intelligent Robot Laboratory of Hangzhou Institute of Technology (HIT) of Xidian University, Xi'an Theory and Application of Discrete Event Dynamic Systems International Science and Technology Cooperation Center, and the Complex Systems International Joint Research Center of Shaanxi Province.

Data Availability Statement: The authors would like to acknowledge the data source: <https://challenge.isic-archive.com/data/> [42,44]. <https://dataverse.harvard.edu/dataset.xhtml?persistentId=doi:10.7910/DVN/FCBUOR> [45] under the licence <https://creativecommons.org/publicdomain/zero/1.0/> under the license: <https://creativecommons.org/publicdomain/zero/1.0/> (all accessed on 1 August 2022).

Conflicts of Interest: The authors declare that there is no conflict of interest.

References

1. Steane, A. Quantum computing. *Rep. Prog. Phys.* **1998**, *61*, 117. [CrossRef]
2. Potok, T.E.; Schuman, C.; Young, S.; Patton, R.; Spedalieri, F.; Liu, J.; Yao, K.T.; Rose, G.; Chakma, G. A study of complex deep learning networks on high-performance, neuromorphic, and quantum computers. *ACM J. Emerg. Technol. Comput. Syst. (JETC)* **2018**, *14*, 19. [CrossRef]
3. Alaminos, D.; Salas, M.B.; Fernández-Gámez, M.A. Quantum computing and deep learning methods for GDP growth forecasting. *Comput. Econ.* **2022**, *59*, 803–829. [CrossRef]
4. Prasantha, H.S.; Dr., S.; Murthy, D.; Madhavi, L. Medical Image Segmentation. *Int. J. Comput. Sci. Eng.* **2010**, *760–762*, 1590–1593.
5. Heimann, T.; Meinzer, H.P. Statistical shape models for 3D medical image segmentation: A review. *Med. Image Anal.* **2009**, *13*, 543–563. [CrossRef] [PubMed]
6. Sohail, A.; Fahmy, M.A.; Khan, U.A. XAI hybrid multi-staged algorithm for routine & quantum boosted oncological medical imaging. *Comput. Part. Mech.* **2022**, 1–11. [CrossRef]
7. Sohail, A. Inference of biomedical data sets using Bayesian machine learning. *Biomed. Eng. Appl. Basis Commun.* **2019**, *31*, 1950030. [CrossRef]
8. Sohail, A.; Arif, F. Supervised and unsupervised algorithms for bioinformatics and data science. *Prog. Biophys. Mol. Biol.* **2020**, *151*, 14–22. [CrossRef]
9. Sohail, A. Genetic algorithms in the fields of artificial intelligence and data sciences. *Ann. Data Sci.* **2021**, 1–12. [CrossRef]
10. Yu, Z.; Gao, H.; Wang, D.; Alnuaim, A.A.; Firdausi, M.; Mostafa, A.M. SEI2RS malware propagation model considering two infection rates in cyber-physical systems. *Phys. A Stat. Mech. Its Appl.* **2022**, *597*, 127207. [CrossRef]
11. Al-Utaibi, K.A.; Sohail, A.; Zafar, A.; Talha, R.; Sait, S.M. AI Optimization of the Exothermic Reaction of Ethylene Oxide with Water. *Biomed. Eng. Appl. Basis Commun.* **2021**, *33*, 2150033. [CrossRef]
12. Al-Utaibi, K.A.; Idrees, M.; Sohail, A.; Arif, F.; Nutini, A.; Sait, S.M. Artificial intelligence to link environmental endocrine disruptors (EEDs) with bone diseases. *Int. J. Model. Simulation, Sci. Comput.* **2021**, *13*, 2250019. [CrossRef]
13. Al-Utaibi, K.A.; Sohail, A.; Arif, F.; Celik, S.; Sait, S.M.; Keskin, D.B. Neural networks to understand the physics of oncological medical imaging. *Biomed. Eng. Appl. Basis Commun.* **2022**, 2250036. [CrossRef]
14. Idrees, M.; Sohail, A. A computational framework and sensitivity analysis for the hormonal treatment of bone. *Clin. Biomech.* **2020**, *73*, 9–16. [CrossRef] [PubMed]
15. Yan, H.; Ma, J.; Feng, Z. Image Segmentation of Pitaya Disease Based on Genetic Algorithm and Otsu Algorithm. *J. Phys. Conf. Ser.* **2021**, *1955*, 012082. [CrossRef]
16. Lakshmi, V.K.; Feroz, C.A.; Merlin, J. Automated Detection and Segmentation of Brain Tumor Using Genetic Algorithm. In Proceedings of the 2018 International Conference on Smart Systems and Inventive Technology (ICSSIT), Tirunelveli, India, 13–14 December 2018.

17. Weese, J.; Lorenz, C. Four Challenges in Medical Image Analysis from an Industrial Perspective. *Med. Image Anal.* **2016**, *33*, 44–49. [[CrossRef](#)]
18. Qiu, Y.; Malomed, B.A.; Mihalache, D.; Zhu, X.; Peng, X.; He, Y. Stabilization of single-and multi-peak solitons in the fractional nonlinear Schrödinger equation with a trapping potential. *Chaos Solitons Fractals* **2020**, *140*, 110222. [[CrossRef](#)]
19. Youssry, A.; El-Rafei, A.; Elramly, S. A quantum mechanics-based framework for image processing and its application to image segmentation. *Quantum Inf. Process.* **2015**, *14*, 3613–3638. [[CrossRef](#)]
20. Aytekin, Ç.; Kiranyaz, S.; Gabbouj, M. Quantum mechanics in computer vision: Automatic object extraction. In Proceedings of the 2013 IEEE International Conference on Image Processing, Melbourne, Australia, 15–18 September 2013; IEEE: New York, NY, USA, 2013; pp. 2489–2493.
21. Sohail, A.; Rees, J.M.; Zimmerman, W.B. Analysis of capillary-gravity waves using the discrete periodic inverse scattering transform. *Colloids Surf. A Physicochem. Eng. Asp.* **2011**, *391*, 42–50. [[CrossRef](#)]
22. Sohail, A.; Yu, Z.; Arif, R.; Nutini, A.; Nofal, T.A. Piecewise differentiation of the fractional order CAR-T cells-SARS-2 virus model. *Results Phys.* **2021**, *33*, 105046. [[CrossRef](#)]
23. Yu, Z.; Sohail, A.; Nofal, T.A.; Tavares, J. Explainability of neural network clustering in interpreting the COVID-19 emergency data. *Fractals* **2021**, *10*, S0218348X22401223. [[CrossRef](#)]
24. Yu, Z.; Abdel-Salam, A.S.G.; Sohail, A.; Alam, F. Forecasting the impact of environmental stresses on the frequent waves of COVID19. *Nonlinear Dyn.* **2021**, *106*, 1509–1523. [[CrossRef](#)] [[PubMed](#)]
25. Arif, R.; Fahmy, M.A.; Amin, N.; Farwa, S.; Sohail, A.; Gepreel, K.A. Crossover behaviour of the Zika virus infection and the delayed immune response. *Results Phys.* **2022**, *41*, 105892. [[CrossRef](#)]
26. Al-Utaibi, K.A.; Sohail, A.; Yu, Z.; Arif, R.; Nutini, A.; Abdel-Salam, A.S.G.; Sait, S.M. Dynamical analysis of the delayed immune response to cancer. *Results Phys.* **2021**, *26*, 104282. [[CrossRef](#)]
27. Yu, Z.; Sohail, A.; Nutini, A.; Arif, R. Delayed Modeling Approach to Forecast the Periodic Behavior of SARS-2. *Front. Mol. Biosci.* **2021**, *7*, 585245. [[CrossRef](#)] [[PubMed](#)]
28. Yu, Z.; Ellahi, R.; Nutini, A.; Sohail, A.; Sait, S.M. Modeling and simulations of CoViD-19 molecular mechanism induced by cytokines storm during SARS-CoV2 infection. *J. Mol. Liq.* **2021**, *327*, 114863. [[CrossRef](#)] [[PubMed](#)]
29. Yu, Z.; Arif, R.; Fahmy, M.A.; Sohail, A. Self organizing maps for the parametric analysis of COVID-19 SEIRS delayed model. *Chaos Solitons Fractals* **2021**, *150*, 111202. [[CrossRef](#)] [[PubMed](#)]
30. Idrees, M.; Sohail, A. Bio-algorithms for the modeling and simulation of cancer cells and the immune response. *Bio-Algorithms Med-Syst.* **2021**, *17*, 55–63. [[CrossRef](#)]
31. Lou, L.; Zeng, H.; Xiong, J.; Li, L.; Gao, W. Schrödinger transform of image: A new tool for image analysis. In *Measurements in Quantum Mechanics*; Books on Demand: Norderstedt, Germany, 2012.
32. Chahid, A.; Serrai, H.; Achten, E.; Laleg-Kirati, T.M. Adaptive method for MRI enhancement using squared eigenfunctions of the Schrödinger operator. In Proceedings of the 2017 IEEE Biomedical Circuits and Systems Conference (BioCAS), Torino, Italy, 19–21 October 2017; IEEE: New York, NY, USA, 2017; pp. 1–4.
33. Benigno, G.B.; Menon, R.S.; Serrai, H. Schrödinger filtering: A precise EEG despiking technique for EEG-fMRI gradient artifact. *NeuroImage* **2021**, *226*, 117525. [[CrossRef](#)] [[PubMed](#)]
34. Yu, Z.; Sohail, A.; Arif, R.; Nutini, A.; Nofal, T.A.; Tunc, S. Modeling the crossover behavior of the bacterial infection with the COVID-19 epidemics. *Results Phys.* **2022**, *39*, 105774. [[CrossRef](#)] [[PubMed](#)]
35. Tang, L.; Tian, L.; Steward, B.L. Color image segmentation with genetic algorithm for in-field weed sensing. *Trans. ASAE* **2000**, *43*, 1019. [[CrossRef](#)]
36. Oliveira, P.; Yamanaka, K. Image Segmentation Using Multilevel Thresholding and Genetic Algorithm: An Approach. In Proceedings of the 2018 2nd International Conference on Data Science and Business Analytics (ICDSBA), Changsha, China, 21–23 September 2018.
37. Yoshinari, K.; Hoshi, Y.; Taguchi, A. Color image enhancement in HSI color space without gamut problem. In Proceedings of the 2014 6th International Symposium on Communications, Control and Signal Processing (ISCCSP), Athens, Greece, 21–23 May 2014; pp. 578–581. [[CrossRef](#)]
38. Selva. Color Image Segmentation Using Genetic Algorithm(Clustering). MATLAB Central File Exchange. 2022. Available online: <https://www.mathworks.com/matlabcentral/fileexchange/64223-color-image-segmentation-using-genetic-algorithm-clustering> (accessed on 1 August 2022).
39. Dhanachandra, N.; Manglem, K.; Chanu, Y.J. Image Segmentation Using K-means Clustering Algorithm and Subtractive Clustering Algorithm. *Procedia Comput. Sci.* **2015**, *54*, 764–771. [[CrossRef](#)]
40. Qureshi, M.N.; Ahamad, M.V. An Improved Method for Image Segmentation Using K-Means Clustering with Neutrosophic Logic. *Procedia Comput. Sci.* **2018**, *132*, 534–540. [[CrossRef](#)]
41. Jha, D.; Smedsrud, P.H.; Riegler, M.A.; Halvorsen, P.; de Lange, T.; Johansen, D.; Johansen, H.D. Kvasir-seg: A segmented polyp dataset. In Proceedings of the International Conference on Multimedia Modeling, Daejeon, Korea, 5–8 January 2020; Springer: Berlin/Heidelberg, Germany, 2020; pp. 451–462.
42. Codella, N.; Rotemberg, V.; Tschandl, P.; Celebi, M.E.; Dusza, S.; Gutman, D.; Helba, B.; Kalloo, A.; Liopyris, K.; Marchetti, M.; et al. Skin lesion analysis toward melanoma detection 2018: A challenge hosted by the international skin imaging collaboration (isic). *arXiv* **2019**, arXiv:1902.03368.

43. Tschandl, P.; Rosendahl, C.; Kittler, H. The HAM10000 dataset, a large collection of multi-source dermatoscopic images of common pigmented skin lesions. *Sci. Data* **2018**, *5*, 180160. [[CrossRef](#)]
44. Codella, N.C.; Gutman, D.; Celebi, M.E.; Helba, B.; Marchetti, M.A.; Dusza, S.W.; Kalloo, A.; Liopyris, K.; Mishra, N.; Kittler, H.; et al. Skin lesion analysis toward melanoma detection: A challenge at the 2017 international symposium on biomedical imaging (isbi), hosted by the international skin imaging collaboration (isic). In Proceedings of the 2018 IEEE 15th International Symposium on Biomedical Imaging (ISBI 2018), Washington, DC, USA, 4–7 April 2018; IEEE: New York, NY, USA, 2018; pp. 168–172.
45. Li, K.; Fathan, M.I.; Patel, K.; Zhang, T.; Zhong, C.; Bansal, A.; Rastogi, A.; Wang, J.S.; Wang, G. Colonoscopy polyp detection and classification: Dataset creation and comparative evaluations. *PLoS ONE* **2021**, *16*, e0255809. [[CrossRef](#)] [[PubMed](#)]